

# GNN-DT: A Graph Neural Network Enhanced Decision Transformer for Efficient Optimization in Dynamic Environments

Stavros Orfanoudakis\*, Nanda Kishor Panda, Peter Palensky and Pedro P. Vergara

Delft University of Technology, Intelligent Electrical Power Grids, Mekelweg 5, Delft, 2628 CD, The Netherlands

## ARTICLE INFO

**Keywords:**  
 Decision Transformer  
 Large Language Models (LLMs)  
 Electric Vehicle (EV)  
 Smart Charging  
 Graph Neural Networks (GNN)

## ABSTRACT

Reinforcement Learning (RL) methods used for solving real-world optimization problems often involve dynamic state-action spaces, larger scale, and sparse rewards, leading to significant challenges in convergence, scalability, and efficient exploration of the solution space. This study introduces GNN-DT, a novel Decision Transformer (DT) architecture that integrates Graph Neural Network (GNN) embedders with a novel residual connection between input and output tokens crucial for handling dynamic environments. By learning from previously collected trajectories, GNN-DT tackles the sparse rewards limitations of online RL algorithms and delivers high-quality solutions in real-time. We evaluate GNN-DT on the complex electric vehicle (EV) charging optimization problem and prove that its performance is superior and requires significantly fewer training trajectories, thus improving sample efficiency compared to existing DT and offline RL baselines. Furthermore, GNN-DT exhibits robust generalization to unseen environments and larger action spaces, addressing a critical gap in prior offline and online RL approaches.

## 1. Introduction

Sequential decision-making problems are critical for efficiently operating a wide array of industries, such as power systems control [Roald et al. \(2023\)](#), logistics optimization [Konstantakopoulos et al. \(2022\)](#), portfolio management [Gunjan and Bhattacharyya \(2023\)](#), and advanced manufacturing processes [Gupta and Gupta \(2020\)](#). However, many practical problems, such as the electric vehicle (EV) charging optimization [Panda and Tindemans \(2024\)](#), are large-scale, have temporal dependencies, and aggregated constraints, often making conventional methods impractical [Bubeck \(2015\)](#). This is especially observed in dynamic environments, where the optimization landscape continuously evolves, requiring real-time solutions.

Reinforcement learning (RL) [Sutton and Barto \(2018\)](#) has been extensively studied for solving optimization problems due to its ability to manage uncertainty, adapt to dynamic environments, and enhance decision-making through trial-and-error [Lan et al. \(2023\)](#); [Zhang et al. \(2023a\)](#). In complex and large-scale scenarios, RL can provide high-quality solutions in real-time compared to traditional mathematical programming techniques that fail to do so [Jaimungal \(2022\)](#). However, RL approaches face significant challenges, such as sparse reward signals that slow learning and hinder convergence to optimal policies [Dulac-Arnold et al. \(2021\)](#). In addition, RL solutions struggle to generalize when deployed in environments different from the one they were trained in, limiting their applicability in real-world scenarios with constantly changing conditions [Wang \(2024\)](#).

Decision Transformers (DT) [Chen et al. \(2021\)](#) is an offline RL algorithm that reframes traditional RL problems as generative sequence modeling tasks conditioned on future

rewards [Zhang et al. \(2023c\)](#). DTs utilize previously collected trajectories to inform decision-making without requiring an environment simulator. By learning from historical data, DTs effectively address the sparse reward issue inherent in online RL, relying on demonstrated successful outcomes instead of extensive trial-and-error exploration. However, the trajectory-stitching mechanism of DT often proves insufficient in dynamic real-world environments, leading to suboptimal policies. Although improved variants such as Q-regularized DT (Q-DT) [Hu et al. \(2024\)](#) incorporate additional constraints for greater robustness, they still face significant challenges in generalizing across non-stationary tasks [Paster et al. \(2024\)](#). Consequently, further architectural advances and training strategies are essential to ensure consistent performance in complex environments.

This study introduces GNN-DT<sup>1</sup>, a novel DT architecture that leverages the permutation-equivariant properties of Graph Neural Networks (GNNs) to handle dynamically changing state-action spaces (i.e., varying numbers of nodes over time) and improve generalization. By generating embeddings that remain consistent under node reordering, GNNs offer a powerful way to capture relational information in complex dynamic environments. Moreover, GNN-DT features a novel residual connection between input and output tokens, ensuring that action outputs are informed by the dynamically learned state embeddings for more robust decision-making. To demonstrate the superior performance of the proposed method, we conduct extensive experiments on the complex multi-objective EV charging optimization problem [Orfanoudakis et al. \(2025a\)](#), which encompasses sparse rewards, temporal dependencies, and aggregated constraints. The main contributions are summarized as follows:

- Introducing a novel DT architecture integrating GNN embeddings, resulting in enhanced sample efficiency,

<sup>1</sup>The code can be found at <https://github.com/StavrosOrf/DT4EVs>.

superior performance, robust generalization to unseen environments, and effective scalability to larger action spaces, demonstrating the critical role of GNNs.

- Demonstrating that online and offline RL baselines, even when trained on diverse datasets (Optimal, Random, Business-as-Usual) with varying sample sizes, perform inferior to GNN-DT when dealing with real-world optimization tasks.
- Proving that both the size and type of training dataset critically influence the learning process of DTs, highlighting the importance of dataset selection. Also, shown that strategically integrating high- and low-quality training data (Optimal & Random datasets) significantly enhances policy learning, outperforming models trained exclusively on single-policy datasets.

## 2. Related Work

### 2.1. Advancements in Decision Transformers

Classic DT encounters significant challenges, including limited trajectory stitching capabilities and difficulties in adapting to online environments. To address these issues, several enhancements have been proposed. The Q-DT [Hu et al. \(2024\)](#) improves the ability to derive optimal policies from sub-optimal trajectories by relabeling return-to-go values in the training data. Elastic DT [Wu et al. \(2024\)](#) enhances classic DT by enabling trajectory stitching during action inference at test time, while Multi-Game DT [Lee et al. \(2024\)](#) advances its task generalization capabilities. The Online DT [Zheng et al. \(2022\)](#); [Villarrubia-Martin et al. \(2023\)](#) extends DTs to online settings by combining offline pretraining with online fine-tuning, facilitating continuous policy updates in dynamic environments. Additionally, adaptations for offline safe RL incorporate cost tokens alongside rewards [Liu et al. \(2023\)](#); [Hong et al. \(2024\)](#). DT has also been effectively applied to real-world domains, such as healthcare [Zhang et al. \(2023c\)](#) and chip design [Lai et al. \(2023\)](#), showcasing its practical utility.

### 2.2. RL for EV Smart Charging

RL algorithms offer notable advantages for EV dispatch, including the ability to handle nonlinear models, robustly quantify uncertainty, and deliver faster computation than traditional mathematical programming [Qiu et al. \(2023\)](#). Popular methods, such as Deep Deterministic Policy Gradient (DDPG) [Jin et al. \(2022\)](#), Soft Actor Critic (SAC) [Jin and Xu \(2021\)](#), and batch RL [Sadeghianpourhamami et al. \(2020\)](#), show promise but often lack formal constraint satisfaction guarantees and struggle to scale with high-dimensional state-action spaces [Yilmaz et al. \(2024\)](#); [Li et al. \(2022\)](#). Safe RL frameworks address these drawbacks by imposing constraints via constrained MDPs, but typically sacrifice performance and scalability [Zhang et al. \(2023b\)](#); [Chen and Shi \(2022\)](#). Multiagent RL techniques distribute complexity across multiple agents, e.g., charging points, stations, or aggregators [Kamrani et al. \(2025\)](#), yet still

encounter convergence challenges and may underperform in large-scale applications. To the best of our knowledge, no study has used DTs to solve the complex EV charging problem, despite DTs' potential to handle sparse rewards effectively.

## 3. Problem Formulation

In this section, an introduction to offline RL and the mathematical formulation of the EV charging optimization problem is presented as an example of what type of problems can be solved by the proposed GNN-DT methodology.

### 3.1. Offline RL

Offline RL aims to learn a policy  $\pi_\theta(a|s)$  that maximizes the expected discounted return  $\mathbb{E}[\sum_{t=0}^{\infty} \gamma^t R(s_t, a_t)]$  without additional interactions with the environment [Levine et al. \(2020\)](#). A Markov Decision Process (MDP) is defined by the tuple  $(S, A, P, R, \gamma)$ , where  $S$  is the state space,  $A$  the action space,  $P$  the transition function,  $R$  the reward function,  $\gamma \in (0, 1]$  the discount factor [Sutton and Barto \(2018\)](#). In the offline setting, a static dataset  $\mathcal{D} = \{(s, a, r)\}$ , collected by a (potentially suboptimal) policy, is provided. DTs leverage this dataset by treating RL trajectories as sequences, learning to predict actions that maximize returns based on previously collected experiences. A key component in DTs is the *return-to-go* (RTG), which for a time step  $t$  can be defined as:  $G_t = \sum_{\tau=t}^T \gamma^{\tau-t} r_\tau$ , representing the discounted cumulative reward from  $t$  until the terminal time  $T$ . Offline RL is particularly beneficial when real-time exploration is costly or impractical, while sufficient historical data are available.

### 3.2. The EV Smart Charging Problem

Working closely with a charge point operator (CPO), it was evident that existing heuristic and mathematical programming charging strategies don't scale efficiently as EV fleets grow. To address this, we designed the state-action space and objectives around real-world operational constraints and assumptions provided by the CPO. We consider a set of  $\mathcal{I}$  charging stations indexed  $i$ , all assumed to be controlled by a CPO over a time window  $\mathcal{T}$ , divided into  $T$  non-overlapping intervals. Since the chargers can be spread around the city, there are charger groups  $w \in \mathcal{W}$ , that can have a lower-level aggregated power limits representing connections to local power transformers. For a given time window, each charging station  $i$  operates a set of  $\mathcal{J}$  non-overlapping charging sessions, denoted by  $\mathcal{J}_i = \{j_{1,i}, \dots, j_{J_i,i}\}$ , where  $j_{j,i}$  represents the  $j^{th}$  charging event at the  $i^{th}$  charging station and  $J_i = |\mathcal{J}_i|$  is the total number of charging sessions seen by charging station  $i$  in an episode. A charging session is then represented as  $j_{j,i} : \{t_{j,i}^a, t_{j,i}^d, \bar{p}_{j,i}, e_{j,i}^*\}$ ,  $\forall j, i$ , where  $t^a, t^d, \bar{p}$  and  $e^*$  represent the arrival time, departure time, maximum charging power, and the desired battery energy level at the departure time. The primary goal is to minimize the total energy cost given by:

$$f_1(p^+, p^-) = \sum_{t \in \mathcal{T}} \sum_{i \in \mathcal{I}} \Delta t (\Pi_t^+ p_{i,t}^+ - \Pi_t^- p_{i,t}^-) \quad (1)$$

**Table 1**

Notation for the EV Charging Optimization Problem

Symbol	Name	Description
<i>Sets</i>		
$\mathcal{T}$	Set of timesteps	Time horizon for optimization
$\mathcal{I}$	Set of charging stations	All EV charging stations
$\mathcal{W}$	Set of charger groups	Chargers grouped by local transformer connections
$\mathcal{J}_i$	Set of charging sessions	Charging sessions at charger $i$
<i>Indexes</i>		
$t$	Timestep index	Discrete time step
$i$	Charger index	Individual EV charging station
$j$	Session index	Charging session at a charger
$w$	Charger group index	Charger groups connected to transformers
<i>Parameters</i>		
$t_{j,i}^a$	Arrival time	Time EV $j$ arrives at charger $i$
$t_{j,i}^d$	Departure time	Time EV $j$ departs charger $i$
$e_{j,i}^*$	Desired battery capacity	Desired battery energy at departure for session $j$ at charger $i$
$e_{j,i}^a$	Arrival battery energy	Battery energy at EV arrival
$\underline{e}_{j,i}, \bar{e}_{j,i}$	Battery limits	Min/max allowable battery energy
$\underline{p}_{j,i}^+, \bar{p}_{j,i}^+$	Charging power limits	Min/max charging power
$\underline{p}_{j,i}^-, \bar{p}_{j,i}^-$	Discharging power limits	Min/max discharging power
$p_t^*$	Total power limit	Desired aggregated power
$\Pi_t^+, \Pi_t^-$	Electricity prices	Prices for charging/discharging at timestep $t$
$\Delta t$	Time interval	Duration of each timestep
$\bar{p}_{w,t}$	Group power limit	Power limit for group $w$ at timestep $t$
<i>Variables</i>		
$p_{i,t}^+, p_{i,t}^-$	Charging/discharging power	Power assigned at charger $i$ , timestep $t$
$\omega_{i,t}^+, \omega_{i,t}^-$	Binary operation indicators	Indicates if charger $i$ charges (+) or discharges (-) at timestep $t$
$e_{j,i,t}$	EV battery energy	Battery level for session $j$ at charger $i$ , timestep $t$
$p_t^{\sum}$	Total aggregated power	Net total power across all chargers at timestep $t$

$p_{i,t}^+$  and  $p_{i,t}^-$  denote the charging or discharging power of the  $i^{th}$  charging station during time interval  $t$ .  $\Pi_t^+$  and  $\Pi_t^-$  are the charging and discharging costs, respectively. Along with minimizing the total energy costs, the CPO also wants the aggregate power of all the charging stations ( $p_t^{\sum} = \sum_{i \in \mathcal{I}} p_{i,t}^+ - p_{i,t}^-$ ) to remain below the set power limit  $p_t^*$ . By doing so, the CPO avoids paying penalties due to overuse of network capacity. Hence, we introduce the penalty:

$$f_2(p^+, p^-) = \sum_{t \in \mathcal{T}} \max\{0, p_t^{\sum} - p_t^*\}, \quad (2)$$

Maintaining the desired battery charge at departure is crucial for EV user satisfaction. We model this behavior as:

$$f_3(p^+, p^-) = \sum_{i \in \mathcal{I}} \sum_{j \in \mathcal{J}_i} \left( \sum_{t=t_{j,i}^a}^{t_{j,i}^d} (p_{i,t}^+ - p_{i,t}^-) - e_{j,i}^* \right)^2 \quad (3)$$

Eq. (3) defines a sparse reward added at each EV departure based on its departure energy level. Building on the objective functions described by Eqs. (1)-(3), the overall EV charging problem is formulated as a mixed integer programming (MIP) problem, subject to lower-level operational constraints (e.g., EV battery, power levels) as detailed below:

$$\begin{aligned} & \max_{p^+, \omega^+, p^-, \omega^-} \sum_{t \in \mathcal{T}} \left[ -100 \max\{0, p_t^{\sum} - p_t^*\} \right. \\ & \quad \left. + \sum_{i \in \mathcal{I}} \left( \Delta t (\Pi_t^+ p_{i,t}^+ \omega_{i,t}^+ - \Pi_t^- p_{i,t}^- \omega_{i,t}^-) \right. \right. \\ & \quad \left. \left. - 10 \sum_{j \in \mathcal{J}_i} \left( \sum_{\tau=t_{j,i}^a}^{t_{j,i}^d} (p_{i,\tau}^+ \omega_{i,\tau}^+ - p_{i,\tau}^- \omega_{i,\tau}^-) - e_{j,i}^* \right)^2 \right) \right] \end{aligned} \quad (4)$$

Subject to:

$$\bar{p}_{w,t} \geq \sum_{i \in \mathcal{W}_i} p_{i,t}^+ \cdot \omega_{i,t}^+ - p_{i,t}^- \cdot \omega_{i,t}^- \quad \forall i, \forall w, \forall t \quad (5)$$

$$e_{j,i} \leq e_{j,i,t} \leq \bar{e}_{j,i} \quad \forall j, \forall i, \forall t \quad (6)$$

$$e_{j,i,t} = e_{j,i,t-1} + (p_{i,t}^+ \cdot \omega_{i,t}^+ + p_{i,t}^- \cdot \omega_{i,t}^-) \cdot \Delta t \quad \forall j, \forall i, \forall t \quad (7)$$

$$e_{j,i,t} = e_{j,i}^a \quad \forall j, \forall i, \forall t | t = t_{j,i}^a \quad (8)$$

$$\underline{p}_{j,i}^+ \leq p_{i,t}^+ \leq \bar{p}_{j,i}^+ \quad \forall j, \forall i, \forall t \quad (9)$$

$$\underline{p}_{j,i}^- \geq \bar{p}_{i,t}^- \geq \bar{p}_{j,i}^- \quad \forall j, \forall i, \forall t \quad (10)$$

$$\omega_{i,t}^+ + \omega_{i,t}^- \leq 1 \quad \forall i, \forall t \quad (11)$$

The multi-objective optimization function in Eq.(4) integrates Eqs. (1)–(3) using experimentally determined coefficients based on practical importance. The power of a single charger  $i$  is modeled using four decision variables,  $p^+ \cdot \omega^+$  and  $p^- \cdot \omega^-$ , where  $\omega^+$  and  $\omega^-$  are binary variables, to differentiate between charging and discharging behaviors and enable charging power to get values in ranges  $0 \cup [\underline{p}^+, \bar{p}^+]$ , and discharging power in  $[\underline{p}^-, \bar{p}^-] \cup 0$ . Eq. (5) defines the locally aggregated transformer power limits  $\bar{p}$  for chargers belonging to groups  $\mathcal{W}_i$ . Eqs. (6)–(8) address EV battery constraints during operation with a minimum and maximum capacity of  $e$ ,  $\bar{e}$ , and energy  $e^a$  at time of arrival  $t^a$ . Equations (9) and (10) impose charging and discharging power limits for every charger-EV session combination. To prevent simultaneous charging and discharging, the binary variables  $\omega^{\text{ch}}$  and  $\omega^{\text{dis}}$  are constrained by (11).

### 3.3. EV Charging MDP

The optimal EV charging problem can be framed as an MDP:  $\mathcal{M} = (S, \mathcal{A}, \mathcal{P}, R)$ , where  $S$  is the state space,  $A$  is the action space,  $P$  is the transition probability function, and  $R$  is the reward function. At any time step  $t$ , the state  $s_t \in S$  is represented by a dynamic graph  $\mathcal{G}_t = (\mathcal{N}_t, \mathcal{E}_t)$ , where  $\mathcal{N}_t$  is the set of nodes and  $\mathcal{E}_t$  is the set of edges. The graph is dynamic since the number of nodes in the state and action graph can vary in each step, because of EVs' arrival and departures. Each node  $n \in \mathcal{N}_t$  has a feature vector  $\mathbf{x}_{n,t} \in \mathbb{R}^d$ , capturing node-dependent information such as power limits and prices. This graph structure [Orfanoudakis et al. \(2025b\)](#) efficiently models evolving relationships among EVs, chargers, and the grid infrastructure. In detail, an EV node's feature vector:

$$\mathbf{x}_t^{\text{ev}} = [\text{SoC}_t, t^d - t, j, i, w] \quad (12)$$

encodes its current state of charge  $\text{SoC}_t \in [0, 1]$ , the remaining steps until departure  $t^d - t$ , and the identifiers  $j$ ,  $i$ , and  $w$  of the charging point, charger, and transformer group to which it is connected. Exact SoC and departure-time information is assumed to be available via ISO 15118 V2G signaling. A charging station (cs) node  $i$  is described by:

$$\mathbf{x}_t^{\text{cs}} = [\bar{p}_{i,j}^+, \bar{p}_{i,j}^-, i], \quad (13)$$

where  $\bar{p}^+$  and  $\bar{p}^-$  are its maximum charging and discharging power and  $i$  its unique identifier. A transformer (tr) node  $w$  has a feature vector:

$$\mathbf{x}_t^{\text{tr}} = [\bar{p}_{w,t}, w], \quad (14)$$

where  $\bar{p}_{w,t}$  denotes its maximum power capacity and  $w$  its identifier, ensuring the policy respects feeder-level constraints. The CPO (system) node aggregates temporal and economic context in

$$\mathbf{x}_t^{\text{cpo}} = \left[ \frac{d}{7}, \sin\left(\frac{h}{48\pi}\right), \cos\left(\frac{h}{48\pi}\right), \Pi_t^+, p_{t-1}^{\Sigma} \right]. \quad (15)$$

Here  $d$  and  $h$  encode day-of-week and hour to capture demand patterns,  $\Pi_t^+$  is the charging price at  $t$ , and  $p_{t-1}^{\Sigma}$  is the previous time step's total power draw, providing feedback for profit-maximizing decisions.

The action space  $\mathbf{a}_t \in \mathcal{A}$  is represented by a dynamic graph  $\mathcal{G}_t^{\mathbf{a}} = (\mathcal{N}_t^{\mathbf{a}}, \mathcal{E}_t^{\mathbf{a}})$ , where nodes  $\mathcal{N}_t^{\mathbf{a}}$  correspond to the decision variables of the optimization problem (e.g., EVs). Each node  $n \in \mathcal{N}_t^{\mathbf{a}}$  represents a single action  $a_{i,t} \in \mathbf{a}_t$ , scaled by the corresponding charger's maximum power limit. For charging,  $a_{i,t} \in [0, 1]$ , and for discharging,  $a_{i,t} \in [-1, 0]$ . The transition function  $\mathcal{P}(s_{t+1} | s_t, \mathbf{a}_t)$  accounts for uncertainties in EV arrivals, departures, energy demands, and grid fluctuations. Finally, the reward function is the same with the objective described in Eq. (4) and is defined as  $R(s_t, \mathbf{a}_t) = f_1 - 100f_2 - 10f_3$  for a single timestep ( $\mathcal{T} = \{t\}$ ). The reward is guiding the policy to maximize cost savings, respect operational constraints, and meet EV driver requirements. While Eqs.(1) and (2) represent individual EV rewards and aggregated EV penalties, respectively. Eq.3 introduces a sparse reward that activates only when an EV departs, thereby creating complex temporal dependencies. The reward function weights were selected after comprehensive experimentation, ensuring the optimal solution of the MIP remains the same while the RL training is balanced between exploration and penalization.

## 4. GNN-based Decision Transformer

The innovative GNN-DT architecture (Fig. 1) efficiently solves optimization problems in complex environments with dynamic state-action spaces by embedding past actions, states, and returns-to-go, using a causal transformer to generate action tokens, and integrating these with current state embeddings to determine final actions within the dynamically changing action space.

### 4.1. Sequence Embeddings

In GNN-DT, each input "modality" is processed by a specialized embedding network. The state graph passes through the *State Embedder*, the action through the *Action Embedder*, and the return-to-go value through a simple Multi-Layer Perceptron (MLP). Compared to standard MLP embedders, GNNs provide embeddings for states and actions invariant to the number of nodes by capturing the graph structure. This design makes GNN-DT more sample-efficient during training and better at generalizing to unseen environments.

In detail, the *State Embedder* consists of  $L$  consecutive Graph Convolutional Network (GCN) [Kipf and Welling \(2016\)](#) layers, which aggregate information from neighboring nodes as follows:

$$\mathbf{x}_t^{(l+1)} = \sigma\left(D^{-1/2}A_tD^{-1/2}\mathbf{x}_t^{(l)}W^{(l)}\right), \quad (16)$$

where  $\mathbf{x}_t^{(l)} \in \mathbb{R}^{N_t \times F_l}$  denotes the node embeddings at layer  $l$  with  $N_t$  number of nodes,  $W^{(l)} \in \mathbb{R}^{F_l \times F_{l+1}}$  are trainable weights,  $\sigma(\cdot)$  is a nonlinear activation (ReLU),  $A_t$  is the

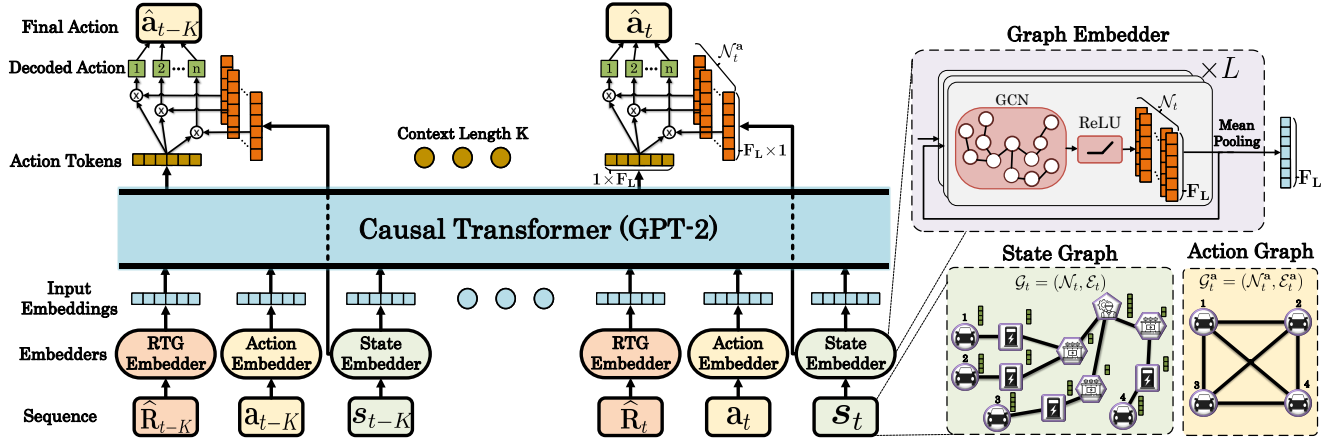


**Figure 1:** Overview of the GNN-DT architecture. The input sequence, comprising return-to-go, action, and state, is processed through specialized embedding modules. The action graph  $G_t^a = (\mathcal{N}_t^a, \mathcal{E}_t^a)$ , with nodes  $\mathcal{N}_t^a \subset \mathcal{N}_t$ , and the state graph  $G_t = (\mathcal{N}_t, \mathcal{E}_t)$  are encoded using GNN-based embedders to produce embeddings of dimension  $F_L$ . These embeddings serve as inputs to a GPT-2-based causal transformer, which predicts the next action token. The predicted action token acts as a decoder, generating actions by multiplying with specific GNN state node embeddings.

adjacency matrix of the state graph  $G_t$ , and  $D$  is the degree matrix for normalization. After the final layer, a mean-pooling operation produces a fixed-size state embedding:  $\tilde{s}_t = \frac{1}{|\mathcal{N}_t|} \sum_{n \in \mathcal{N}_t} \mathbf{x}_{n,t}^{(L)}$ , where  $\mathbf{x}_{n,t}^{(L)}$  is the embedding of node  $n$  at the  $L$ -th layer. This pooling step ensures that the state embedding is invariant to the number of nodes in the graph, enabling the architecture to scale with any number of EVs or chargers. Similarly, the *Action Embedder* processes the action graph  $G_t^a = (\mathcal{N}_t^a, \mathcal{E}_t^a)$  through  $C$  GCN layers followed by mean pooling, producing the action embedding  $\tilde{\mathbf{a}}_t$ . All embedding vectors (states, actions, or the return-to-go value) have the same dimensions. This design leverages the dynamic and invariant nature of GCN-based embeddings, allowing the DT to handle variable-sized graphs.

## 4.2. Decoding Actions

Once the embedding sequence of length  $K$  is constructed<sup>2</sup>, it is passed through the causal transformer GPT-2 to produce a fixed-size output vector  $\mathbf{y}_t \in \mathbb{R}^{F_L}$  for each step. Because DT architectures inherently generate outputs of fixed dimensions, an additional mechanism is required to manage dynamic action spaces. To address this, GNN-DT implements a residual connection that merges the final GCN layer embeddings  $\mathbf{x}_t^{(L)}$  with the transformer output  $\mathbf{y}_t$  for every step of the sequence. Specifically, for each node  $n \in \mathcal{N}_t^a$ , we retrieve its corresponding state embedding  $\mathbf{x}_{n,t}^{(L)} \in \mathbb{R}^{1 \times F_L}$  and multiply it with the transformer output token  $\mathbf{y}_t \in \mathbb{R}^{1 \times F_L}$ , yielding the final action for node  $n$ :  $\hat{\mathbf{a}}_{n,t} = \mathbf{y}_t^\top \cdot \mathbf{x}_{n,t}^{(L)}$ . By repeating for every step  $t$  and every node  $n \in \mathcal{N}_t^a$  the final action vector  $\hat{\mathbf{a}}_t$  is generated. This design allows the model to maintain a fixed-size output from the DT while dynamically adapting to any number of nodes (and hence actions). It effectively combines the

high-level context learned by the transformer with the node-specific state information captured by the GNN, enabling robust, scalable decision-making even as the graph structure changes.

## 4.3. Training: Action Masking and Loss Function

The proposed GNN-DT model is trained via supervised learning using an offline trajectory dataset [Chen et al. \(2021\)](#), similarly to offline RL. Specifically, the GPT-2 model is initialized with its default pre-trained weights, which are subsequently fine-tuned end-to-end for the EV charging optimization task. In GNN-DT, the learning of infeasible actions, such as charging an unavailable EV, is avoided through action masking. At each time step  $t$ , a mask vector  $\mathbf{m}_t$ , which has the same dimension as  $\mathbf{a}_t$ , is generated with zeros marking invalid actions and ones marking valid actions. For example, an action is invalid when the  $a_{i,t} \neq 0$  and no EV is connected at charger  $i$ . The mean squared error between the predicted actions  $\hat{\mathbf{a}}_t$  and ground-truth actions  $\mathbf{a}_t$  from expert or offline trajectories is employed as the loss function. For a window of length  $K$  ending at time  $t$ , training loss is defined as:

$$\mathcal{L} = \frac{1}{K} \sum_{\tau=t-K}^t \|(\hat{\mathbf{a}}_\tau - \mathbf{a}_\tau) \circ \mathbf{m}_\tau\|^2. \quad (17)$$

By incorporating the mask into the loss calculation (elementwise multiplication), a focus solely on valid actions is enforced, thereby preserving meaningful gradient updates.

## 5. Experimental Setup

The dataset generation and the evaluation experiments are conducted using the EV2Gym simulator [Orfanoudakis et al. \(2025a\)](#), which leverages real-world data distributions, including EV arrivals, EV specifications, electricity prices, etc. This setup ensures a realistic environment where the

<sup>2</sup>During inference the action ( $\mathbf{a}_t$ ) and RTG ( $\hat{\mathbf{R}}_t$ ) of the last step  $t$  are filled with zeros as they are not known.

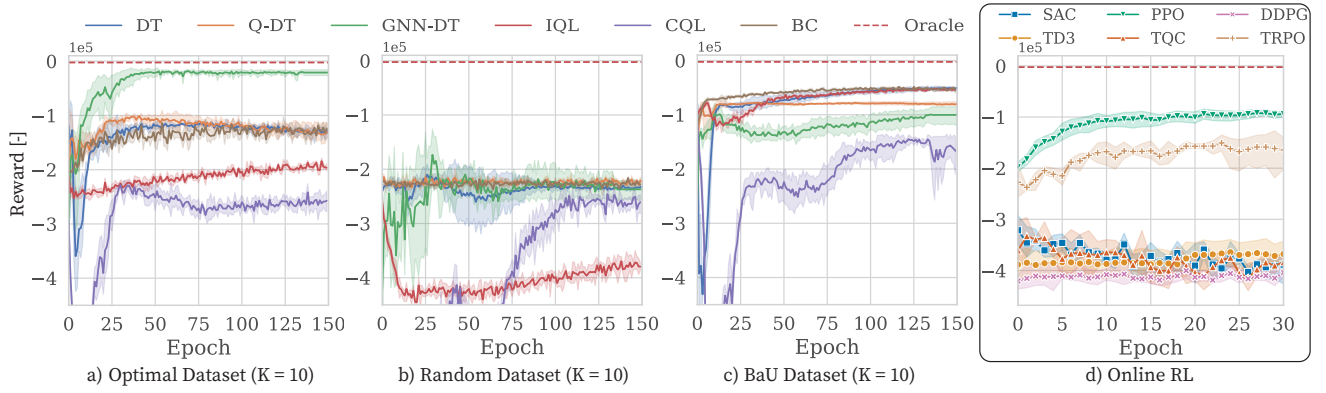


Figure 2: Training performance comparison for online and offline RL algorithms.

Table 2

Algorithm hyperparameters for small- and large-scale settings.

Hyperparameter	Small scale	Large scale
Batch size	128	64
Learning rate	$10^{-4}$	$10^{-4}$
Weight decay	$10^{-4}$	$10^{-4}$
Steps per iteration	1000	3000
Decoder layers	3	3
Attention heads	4	4
Embedding dimension	128	256
GNN embedder feat. dim.	16	16
GNN hidden dimension	32	64
GCN layers	3	3
Epochs	250	400
CPU memory (GB)	8	40
Time limit (h)	10	46

state and action spaces accurately reflect real charging stations' operational complexity. A scenario with 25 chargers is chosen, allowing up to 25 EVs to be connected simultaneously. In this configuration, the action vector has up to 25 variables (one per EV), while the state vector contains around 150 variables describing EV statuses, charger conditions, power transformer constraints, and broader environmental factors. Consequently, the resulting optimization problem is in the moderate-to-large scale range, reflecting the key complexities of real-world EV charging. Each training procedure is repeated 10 times with distinct random seeds to ensure statistically robust findings. All reported rewards represent the average performance over 50 evaluation scenarios, each featuring different configurations (electricity prices, EV behavior, power limits, etc.). Training was carried out on an NVIDIA A10 GPU paired with 11 CPU cores and 80 GB of RAM, using the AdamW optimizer and a LambdaLR scheduler. Baseline RL agents converged in 2–5 hours, while the proposed GNN-DT required up to 10 hours of training. Default hyperparameters were used for all baseline RL methods; Table 2 lists the full set of hyperparameters employed to train the DTs.

### 5.1. Dataset Generation

Offline RL algorithms, including DTs, can learn policies from trajectories without needing online interaction with the environment. Consequently, the quality of the gathered training trajectories has a substantial impact on the learning process. In this work, three distinct strategies were used to generate trajectories:

- **Random Actions:** Uniformly sampled actions in the range  $[-1, 1]$  were applied to the simulator.
- **Business-as-Usual (BaU):** A Round Robin charging policy commonly employed by CPOs, which sequentially allocates charging power among EVs to balance fairness and efficiency.
- **Optimal Policies:** Optimal solutions derived from solving offline the mathematical problem described in Section 3.2 for randomly generated scenarios.

Each trajectory consists of 300 state-action-reward-action mask tuples, with each timestep representing a 15-minute interval, resulting in a total of three simulated days. This combination of random, typical, and expert data provides a comprehensive basis for evaluating how GNN-DT learns from diverse offline trajectories.

## 6. Experiments

In this section, a comprehensive set of experiments is presented to evaluate the proposed method's performance, both during training and under varied test conditions. Different dataset types and sample sizes are examined to determine their impact on learning efficiency and convergence.

### 6.1. Training Performance

Fig. 2 compares the proposed GNN-DT against multiple baselines, including the classic DT Chen et al. (2021) and Q-DT Hu et al. (2024), which both rely on flattened state representations due to their inability to directly process graph-structured data. In these baseline methods, empty chargers and unavailable actions are replaced by zeros, so the action vector is always the same size. Several well-known online

**Table 3**

Comparison of maximum episode rewards ( $\times 10^5$ ) for baselines and GNN-DT across datasets and context lengths ( $K$ ). **Bold** indicates the highest value within each dataset and  $K$  category.

Dataset	Avg. Training Dataset Reward	K=2			K=10		
		DT	Q-DT	GNN-DT	DT	Q-DT	GNN-DT
Random 100		-1.91	-1.97	<b>-0.82</b>	-2.12	-2.09	-1.16
Random 1000	$-2.37 \pm 0.39$	-1.93	-2.04	-0.86	-2.11	-2.01	-1.18
Random 10000		-1.76	-2.04	-1.25	-1.81	-1.98	<b>-0.98</b>
BaU 100		-0.79	-0.74	<b>-0.59</b>	-0.79	-0.72	-0.56
BaU 1000	$-0.67 \pm 0.07$	-0.71	-0.66	-0.65	-0.64	-0.71	-0.57
BaU 10000		-0.69	-0.66	-0.66	<b>-0.44</b>	-0.74	-0.53
Optimal 100		-0.67	-0.91	-0.15	-1.12	-0.90	-0.14
Optimal 1000	$-0.01 \pm 0.01$	-0.63	-0.67	-0.10	-0.87	-0.86	-0.09
Optimal 10000		-0.63	-0.80	<b>-0.04</b>	-0.72	-0.90	<b>-0.07</b>

RL algorithms from the Stable-Baselines-3 [Raffin et al. \(2021\)](#) framework are evaluated, such as SAC, DDPG, Twin Delayed DDPG (TD3), Trust Region Policy Optimization (TRPO), Proximal Policy Optimization (PPO), and Truncated Quantile Critics (TQC). Also, offline RL algorithms from D3RLPY [Seno and Imai \(2022\)](#), namely Implicit Q-Learning (IQL), Conservative Q-Learning (CQL), and Behavioral Cloning (BC), are also included. The offline RL algorithms (IQL, CQL, BC, DT, Q-DT, and GNN-DT) are trained on three datasets (*Optimal*, *Random*, and *BaU*), each comprising 10.000 trajectories. A red dotted line marks the optimal reward, which represents the experimental maximum achievable reward obtained by solving the deterministic MIP knowing the future (*Oracle*) defined in Eq. 4. This oracle reward serves as an upper bound and helps contextualize the relative performance of each method. It is important to note that the EV smart charging problem requires real-time (1-5 min intervals) optimization solutions for large-scale, highly stochastic scenarios, where metaheuristic algorithms, stochastic optimization, and model predictive control methods fail due to computational constraints. By contrast, once trained (over 2–24 hours), RL agents can deliver real-time charging schedules on an ordinary computer in milliseconds.

In Figs. 2.a-c, the DT-based approaches use a context length  $K = 10$ . As expected, the *Optimal* dataset provides the highest-quality information, enabling GNN-DT to converge rapidly toward near-oracle performance, while classic DT, Q-DT, and the other offline RL algorithms lag far behind, showcasing GNN-DT's improved sample efficiency. With the *Random* dataset, the limited quality of data leads all methods to plateau at lower reward values, although GNN-DT still surpasses the other baselines. An intriguing behavior is observed with the *BaU* dataset, where classic DT, BC, and IQL converge at rewards exceeding those of GNN-DT. In contrast, the online RL algorithms displayed in Fig. 2.d struggle to achieve comparable improvements, suggesting that pure online exploration is insufficient for solving this

complex EV charging optimization problem with sparse rewards. In the rest of this section, we omit the online and offline RL baselines, as their performance is substantially inferior to that of DT, Q-DT, and GNN-DT.

## 6.2. Dataset Impact

In Table 3, the maximum episode reward is compared for small, medium, and large datasets (100, 1.000, and 10.000 trajectories), under two different context lengths ( $K = 2$  and  $K = 10$ ). The left side of Table 3 reports the dataset type, the number of trajectories, and the average reward in each dataset. All baselines achieve performance above the *Random* dataset's average reward. However, only GNN-DT consistently approaches the *Optimal* dataset's performance, reaching as close as  $-0.04 \times 10^5$  compared to the  $-0.01 \times 10^5$  optimal reward. This advantage becomes especially evident at the largest dataset size (10.000 trajectories), highlighting the benefits of the graph-based embedding layer. Overall, GNN-DT outperforms the baselines across all datasets and both context lengths, with the single exception of the *BaU* dataset at  $K = 10$ . Interestingly, a larger context window does not always translate into higher rewards, potentially due to the problem setting. Similarly, the dataset size appears to have minimal impact on Q-DT, whereas DT and GNN-DT generally improve with more trajectories. These findings underscore that both the quality and quantity of offline data, coupled with the GNN-DT architecture, are key to achieving superior performance.

## 6.3. Enhancing Training Datasets

The previous section highlighted that the quality of trajectories in the training dataset is the most influential factor for achieving high performance. In this section, we explore whether creating new datasets by mixing existing ones can further improve performance. The *Optimal* and *Random* datasets are combined in different proportions, as summarized in Table 4. A noteworthy result is that supplementing the *Optimal* dataset with “less useful” (*Random*)

**Table 4**

Maximum reward of GNN-DT trained on merged *Optimal* and *Random* datasets for  $K = 2$  and  $K = 10$ . Performance improves despite lower average training rewards, highlighting the importance of dataset diversity. Highest rewards per  $K$  are highlighted with **bold**.

Dataset	Total Traj.	Avg. Dataset Reward	GNN-DT Reward ( $\times 10^5$ )	
			K=2	K=10
Random (Rnd.) 100%	1000	$-2.37 \pm 0.39$	-0.863	-1.187
Opt. 25% + Rnd. 75%	1000	$-1.78 \pm 1.07$	-0.045	<b>-0.020</b>
Opt. 50% + Rnd. 50%	1000	$-1.18 \pm 1.19$	<b>-0.021</b>	-0.040
Opt. 75% + Rnd. 25%	1000	$-0.60 \pm 1.03$	-0.073	-0.057
Optimal (Opt.) 100%	1000	$-0.01 \pm 0.01$	-0.108	-0.099

**Table 5**

Maximum reward of GNN-DT trained on merged BaU-*Random* datasets for  $K = 2$  and  $K = 10$ . The bold indicates the training dataset with the highest evaluation reward.

Dataset	Total Traj.	Avg. Dataset Reward	GNN-DT Reward ( $\times 10^5$ )	
			K=2	k=10
Random (Rnd.) 100%	1000	$-2.37 \pm 0.39$	-0.863	-1.187
BaU 25% + Rnd. 75%	1000	$-1.93 \pm 0.80$	-0.578	-0.461
BaU 50% + Rnd. 50%	1000	$-1.51 \pm 0.87$	-0.665	<b>-0.447</b>
BaU 75% + Rnd. 25%	1000	$-1.09 \pm 0.76$	<b>-0.421</b>	-0.471
BaU 100%	1000	$-0.01 \pm 0.01$	-0.654	-0.572

trajectories consistently boosts performance. In particular, GNN-DT with  $K = 10$ , trained on a mix of 250 *Optimal* and 750 *Random* trajectories, achieves near-oracle results, deviating by only  $-0.001 \times 10^5$  from the optimal reward. A similar trend emerges when blending *BaU* and *Random* datasets shown in Table 5. While the *BaU* dataset alone performs worse than the *Optimal* dataset, mixing it with *Random* data still yields improvements, with the 75% *BaU* and 25% *Random* combination showing the best results. Overall, these findings indicate that carefully integrating high- and lower-quality data can enhance policy learning beyond what purely *Optimal* or purely *Random* datasets can provide.

#### 6.4. Impact of larger context lengths (K)

Fig. 3 demonstrates that the context length  $K$  plays a key role in the performance of GNN-DT, with diminishing returns beyond a certain point. For high-quality datasets like *Optimal*, moderate context lengths ( $K = 5$  to  $K = 10$ ) yield the best results, while larger  $K$  values do not improve performance significantly. For suboptimal datasets like *BaU* and *Random*, the performance is lower overall, and longer context lengths seem to offer meaningful improvements, particularly when using the *BaU* dataset. Thus, selecting an appropriate context length is crucial for achieving better performance, while the quality of the dataset remains the most influential factor.

#### 6.5. Component Ablation Study

To better understand the contribution of each architectural component, we conduct an ablation study that systematically removes or replaces elements of our model and then trains the model on the *Optimal* and *Mixed* (Opt.25%

+Rand.75%). The results in Table 6 reveal that neither a plain DT nor a DT augmented solely with a state-GNN sub-module achieves competitive performance. Notably, adding the residual connection atop the state-GNN leads to a significant improvement, from  $-0.77 \times 10^5$  to  $-0.16 \times 10^5$  on the *Mixed* dataset, demonstrating its importance for effective credit assignment over dynamic inputs. Removing action masking or replacing the GCN module with a Graph Attention Network (GAT) Veličković et al. (2018) similarly degrades performance, indicating that each component provides distinct and complementary benefits. Ultimately, only the full GNN-DT architecture achieves strong performance across both the *Mixed* and *Optimal* datasets.

#### 6.6. Average Results of EV Charging.

Table 7 shows a comparison of key EV charging metrics for the 25-station problem after 100 evaluations, including heuristic algorithms, Charge As Fast as Possible (CAFAP) and *BaU*, and DT variants with the optimal solution, which assumes future knowledge.

The performance of the proposed algorithms was assessed using several evaluation metrics. For example, user satisfaction [%] captures the extent to which the state of charge at departure ( $e_{j,t^d}$ ) of each electric vehicle  $j \in \mathcal{J}$  meets its target  $e_j^*$ , thus defined as:

$$\text{User Satisfaction [%]} = \frac{1}{|\mathcal{J}|} \sum_{j \in \mathcal{J}} \left( \frac{e_{j,t^d}}{e_j^*} \right) \cdot 100\%. \quad (18)$$

Energy charged [kWh] was measured as the total amount of energy delivered to the vehicles during the charging sessions, while energy discharged [kWh] was quantified as the energy returned from vehicles to the grid. Power violations

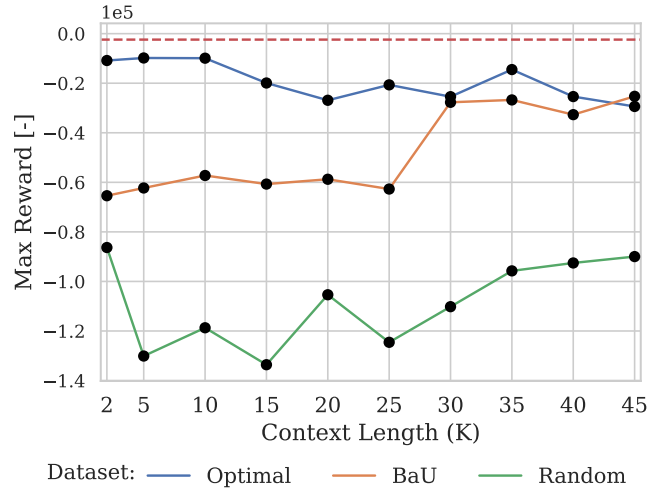


Figure 3: GNN-DT performance for larger context lengths (K).

Table 6

Average reward trained over 5 runs with different seeds for *Optimal* and *Mixed* datasets.

DT	State GNN	Action GNN	Res. Con.	Action Mask	Optimal ( $\times 10^5$ )	Mixed ( $\times 10^5$ )
✓	$\times$	$\times$	$\times$	$\times$	$-0.69 \pm 0.03$	$-0.95 \pm 0.39$
✓	GCN	$\times$	$\times$	$\times$	$-0.71 \pm 0.02$	$-0.77 \pm 0.17$
✓	GCN	$\times$	✓	$\times$	$-0.18 \pm 0.03$	$-0.16 \pm 0.07$
✓	GCN	GCN	✓	$\times$	$-0.11 \pm 0.03$	$-0.12 \pm 0.04$
✓	GAT	GAT	✓	✓	$-0.14 \pm 0.07$	$-0.15 \pm 0.06$
✓	GCN	GCN	✓	✓	<b><math>-0.09 \pm 0.02</math></b>	<b><math>-0.10 \pm 0.04</math></b>

[kW] were tracked to identify instances in which operational limits were exceeded, ensuring system feasibility. Finally, the overall charging cost [€] was evaluated by accounting for the time-varying electricity prices during charging and discharging periods, thus reflecting the economic performance of the strategy.

GNN-DT shows remarkable performance, achieving a close approximation to the optimal solution, particularly in user satisfaction ( $99.3\% \pm 0.03\%$ ) and power violation ( $21.7 \pm 22.8$  kW). It outperforms both BaU and DT variants in terms of energy discharged, power violation, and costs. Notably, GNN-DT performs well even compared to Q-DT, while maintaining competitive execution time, albeit slightly slower than the simpler models. The results underscore the effectiveness of GNN-DT in managing complex EV charging tasks, demonstrating its potential for real-world applications where future knowledge is not available.

## 6.7. Illustrative Example of EV Charging

With the models trained, we proceed to compare the behavior of the best baseline models trained (DT, Q-DT, GNN-DT) against the heuristic BaU algorithm in an EV charging scenario. Fig. 4a presents the SoC progress for three EVs connected one after the other to a single charger throughout the simulation, while Fig. 4b shows the actions

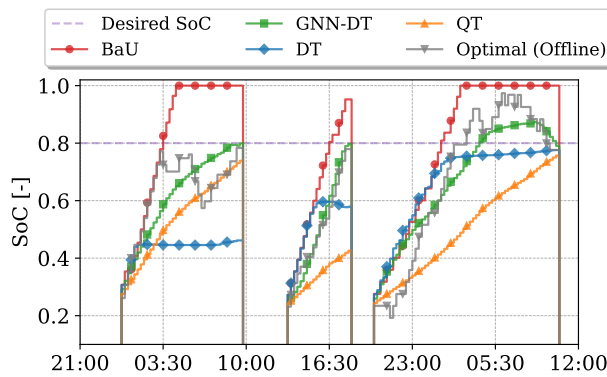
of all chargers taken by each algorithm. At the beginning of the simulation, EVs arrive at the charging station with unknown initial SoCs. Upon connection, they communicate their departure times and desired SoC levels to the CPO. Leveraging this information, along with real-time electricity price signals and power constraints, each algorithm determines optimal charging and discharging actions.

In Fig. 4a, the heuristic BaU algorithm consistently overcharges the EVs, often exceeding the desired SoC levels. In contrast, both DT and Q-DT fail to satisfy the desired SoC. Conversely, GNN-DT successfully achieves the desired SoC for all EVs, closely mirroring the behavior of the optimal algorithm. This demonstrates GNN-DT's ability to precisely control charging based on dynamic state information. Fig. 4b provides further insights into the actions taken by each algorithm. The optimal solution primarily employs maximum charging or discharging power, since it knows the future. In comparison, GNN-DT exhibits a more refined approach, modulating charging power within a range of -6 to 11 kW. Baseline DT and Q-DT display a narrower range of actions, limiting their ability to optimize the charging schedules and adapt to varying conditions. These results underscore the superior capability of GNN-DT in managing the complexities of EV charging dynamics.

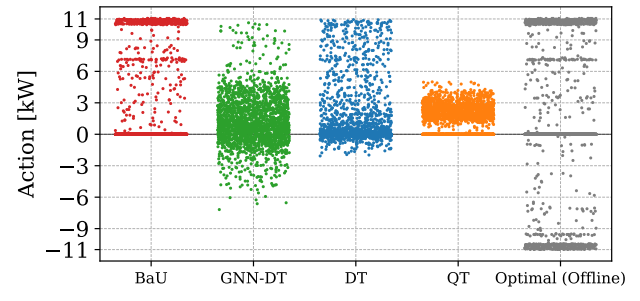
**Table 7**

Comparison of key EV charging metrics for the 25-station problem after 100 evaluations, for heuristic algorithms (CAFAP & BaU) and DT variants with the optimal solution, which assumes future knowledge.

Algorithm	Energy Charged [MWh]	Energy Discharged [MWh]	User Satisfaction [%]	Power Violation [kW]	Costs [€]	Reward [-10 <sup>5</sup> ]	Exec. Time [sec/step]
CAFAP	1.3 ±0.2	0.00 ±0.00	100.0 ±0.0	1289.2 ±261.8	-277 ±165	-1.974 ±0.283	0.001
BaU	1.3 ±0.2	0.00 ±0.00	99.9 ±0.2	10.5 ±9.4	-255 ±156	-0.679 ±0.067	0.001
DT	0.9 ±0.1	0.03 ±0.01	94.4 ±1.6	58.7 ±28.3	-173 ±104	-0.462 ±0.093	0.006
Q-DT	1.0 ±0.1	0.00 ±0.00	93.6 ±2.1	20.1 ±21.4	-187 ±113	-0.665 ±0.135	0.010
<b>GNN-DT (Ours)</b>	0.9 ±0.1	0.19 ±0.03	99.3 ±0.2	21.7 ±22.8	-142 ±89	-0.027 ±0.023	0.023
Optimal (Offline)	1.9 ±0.2	1.08 ±0.19	99.1 ±0.2	2.0 ±4.6	-119 ±84	-0.020 ±0.015	-



(a) EVs' battery level progression over time.



(b) Charger Actions

**Figure 4:** Comparison of smart charging algorithms for a single simulation day.

## 6.8. Generalization and Scalability Analysis

Evaluating the generalization of RL models across varying state transition probabilities is crucial for ensuring consistent performance under diverse conditions Wang et al. (2020). To evaluate the generalization capabilities of GNN-DT, three additional environments with different state transition probabilities are designed. The key environment variables that directly impact the state transition dynamics are visualized in Figure 5. In detail, Figure 5a–d presents the probability distributions of EV arrival time, departure time, duration of stay, and state of SoC at arrival across four scenarios: the original training environment and environments with small, medium, and extreme variations. These plots help quantify the extent of variation in each case. Additionally, Figure 5e illustrates the temporal distribution of the power limit in each scenario, providing further insight into the differences in environment configuration.

In Fig. 6a, the generalization capabilities of GNN-DT and other baselines are assessed in environments with small, medium, and extreme variations in state transition probabilities. While the baseline methods experience significant performance drops as the evaluation environment deviates from the training setting, GNN-DT maintains strong performance across all scenarios. This highlights the critical role of GNN-based embeddings in improving model robustness and generalization. A key advantage of the GNN-DT

architecture, not present in classic DTs, is its invariance to problem size, i.e., the same RL agent can be applied to both smaller and larger-scale environments. Fig. 6b illustrates the scalability and generalization performance of GNN-DT compared to the BaU algorithm and Optimal policy. GNN-DT, trained on a 25-charger setup, was tested on 5, 50, 75, and 100-charger environments. While its performance predictably declines at larger scales, since it wasn't trained on them, it still outperforms the BaU heuristic, demonstrating robustness to problem-size variation. Training GNN-DT on a mix of charger numbers could potentially further improve its adaptability.

The scalability and effectiveness of GNN-DT were tested when trained on a significantly larger optimization problem involving 250 charging stations. In this scenario, the model must handle up to 250 action variables per step and over 1,000 state variables, which include critical information such as power limits and battery levels. The results presented in Table 8 demonstrate that GNN-DT shows promise for addressing more complex optimization tasks. However, the model requires a substantial increase in both the number of training trajectories and memory resources to maintain efficiency, highlighting a well-known limitation of DT-based approaches. Scaling the problem 10 $\times$  roughly multiplies GPU memory usage, e.g. storing 3,000 trajectories takes  $\approx$  2 GB for 25 chargers versus  $\approx$  20 GB for 250. While

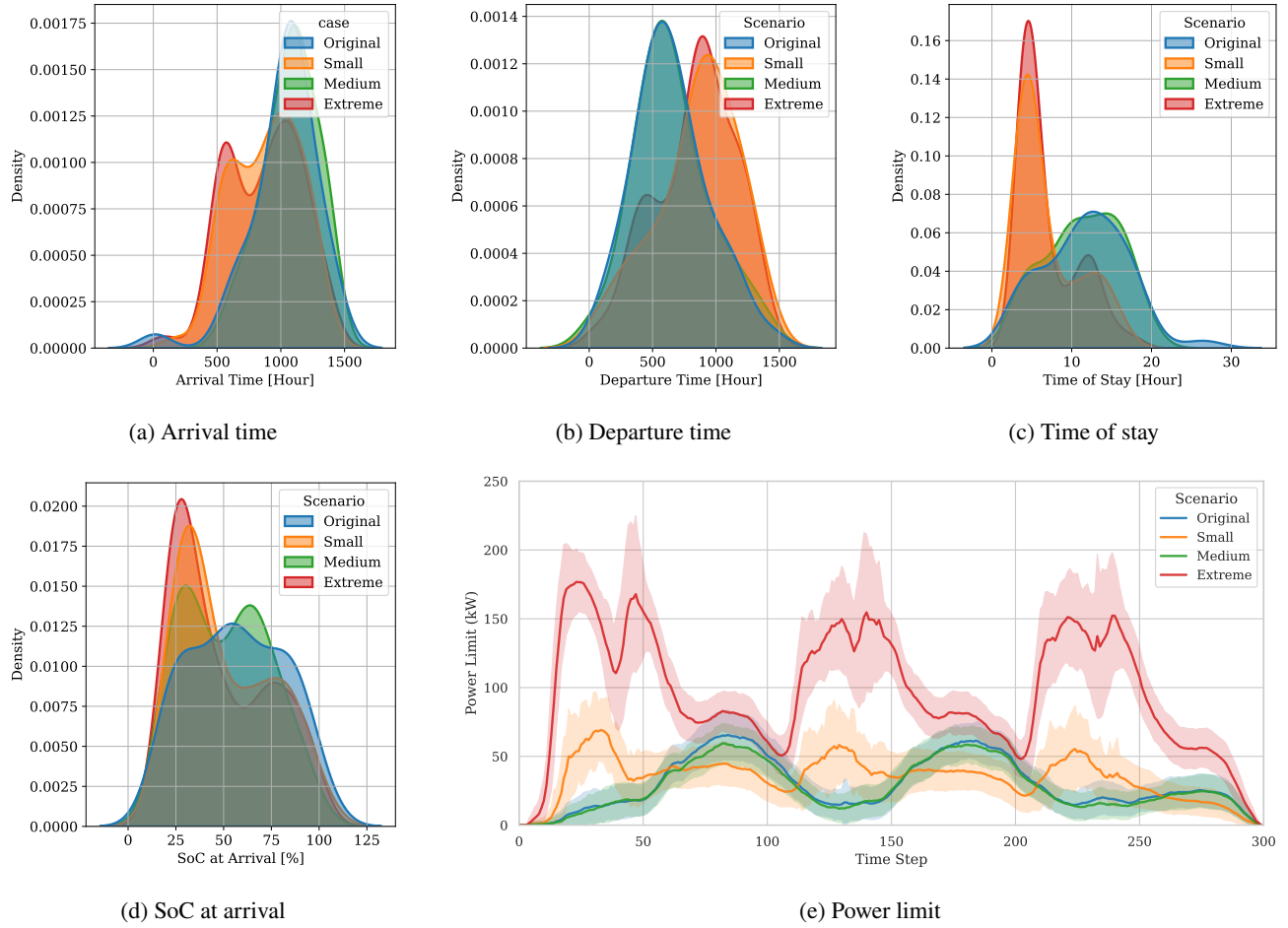


**Figure 5:** Overview of the five key state transition variables across different scenarios: (a) arrival time, (b) departure time, (c) power limit, (d) state of charge upon arrival, and (e) time of stay.

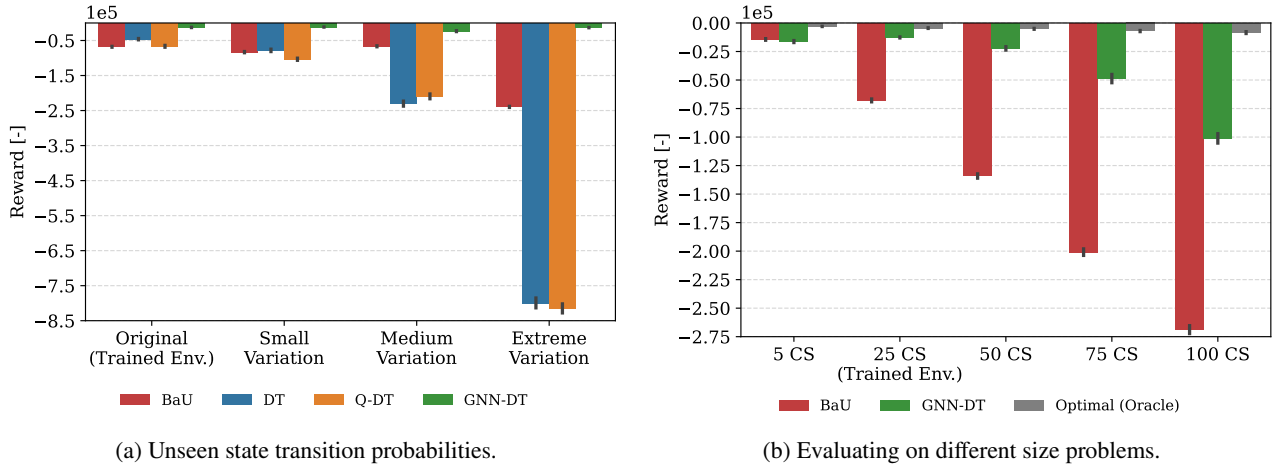


**Figure 6:** Generalization performance of the proposed model, depicting the average rewards achieved across 100 randomly generated scenarios in previously unseen environments.

this can bottleneck large-scale training, parallelization and mini-batching mitigate it, and overall compute scales with the transformer's context length  $K$  (see Fig. 3), pointing to interesting directions for very large problem graphs as future work.

## 7. Conclusions

In this work, we introduced a novel DT-based architecture, GNN-DT, which incorporates GNN embedders to

**Table 8**

Max. reward of GNN-DT in a large-scale EV charging optimization task with 250 chargers.

	Total Trajectories	Avg. Dataset Reward	GNN-DT Reward
Random	3000	$-22.39 \pm 1.49$	-9.34
BaU	3000	$-6.67 \pm 0.32$	-4.23
Optimal	3000	$-0.08 \pm 0.03$	<b>-0.27</b>

significantly enhance sample efficiency and overall performance in the sequential decision-making problem of EV charging. Through extensive evaluation across various datasets, including optimal, random, and BaU, we demonstrated that traditional DTs, online and offline RL algorithms fail to effectively solve real-world problems without specialized embeddings. We further show that both the size and quality of input trajectories critically impact the training process, underscoring the importance of carefully selecting datasets for effective learning. Finally, by leveraging the power of GNN embeddings, GNN-DT improved the model's ability to generalize in previously unseen environments and handle large, complex action spaces. These contributions demonstrate GNN-DT's potential to address complex dynamic optimization challenges beyond EV charging.

## Acknowledgements

The study was partially funded by the DriVe2X research and innovation project from the European Commission with grant numbers 101056934. The authors acknowledge the use of computational resources of the DelftBlue supercomputer, provided by Delft High Performance Computing Centre (<https://www.tudelft.nl/dhpc>). This work used the Dutch national e-infrastructure with the support of the SURF Cooperative using grant no. EINF-5716.

## CRedit authorship contribution statement

**Stavros Orfanoudakis:** Conceptualization, Methodology, Software, Writing - Original Draft, Writing - Review & Editing. **Nanda Kishor Panda:** Conceptualization, Writing - Original Draft, Writing - Review & Editing. **Peter Palensky:** Supervision, Funding acquisition. **Pedro P. Vergara:** Conceptualization, Supervision, Funding acquisition, Writing - Review & Editing.

## References

Bubeck, S., 2015. Convex Optimization: Algorithms and Complexity. *Now Foundations and Trends*. doi:[10.1561/2200000050](https://doi.org/10.1561/2200000050).

Chen, G., Shi, X., 2022. A deep reinforcement learning-based charging scheduling approach with augmented lagrangian for electric vehicle. [arXiv:2209.09772](https://arxiv.org/abs/2209.09772).

Chen, L., Lu, K., Rajeswaran, A., Lee, K., Grover, A., Laskin, M., Abbeel, P., Srinivas, A., Mordatch, I., 2021. Decision transformer: Reinforcement learning via sequence modeling. [arXiv:2106.01345](https://arxiv.org/abs/2106.01345).

Dulac-Arnold, G., Levine, N., Mankowitz, D.J., Li, J., Paduraru, C., Gowal, S., Hester, T., 2021. Challenges of real-world reinforcement learning: definitions, benchmarks and analysis. *Machine Learning* 110, 2419–2468. URL: <https://doi.org/10.1007/s10994-021-05961-4>, doi:[10.1007/s10994-021-05961-4](https://doi.org/10.1007/s10994-021-05961-4).

Gujan, A., Bhattacharyya, S., 2023. A brief review of portfolio optimization techniques. *Artificial Intelligence Review* 56, 3847–3886.

Gupta, K., Gupta, M.K. (Eds.), 2020. Optimization of Manufacturing Processes. Springer Series in Advanced Manufacturing.

Hong, K., Li, Y., Tewari, A., 2024. A primal-dual-critic algorithm for offline constrained reinforcement learning, in: Dasgupta, S., Mandt, S., Li, Y. (Eds.), *Proceedings of The 27th International Conference on Artificial Intelligence and Statistics*, PMLR. pp. 280–288. URL: <https://proceedings.mlr.press/v238/hong24a.html>.

Hu, S., Fan, Z., Huang, C., Shen, L., Zhang, Y., Wang, Y., Tao, D., 2024. Q-value regularized transformer for offline reinforcement learning, in: *Forty-first International Conference on Machine Learning*. URL: <https://openreview.net/forum?id=ojtddicekd>.

Jaimungal, S., 2022. Reinforcement learning and stochastic optimisation. *Finance and Stochastics* 26, 103–129. URL: <https://doi.org/10.1007/s00780-021-00467-2>, doi:[10.1007/s00780-021-00467-2](https://doi.org/10.1007/s00780-021-00467-2).

Jin, J., Xu, Y., 2021. Optimal policy characterization enhanced actor-critic approach for electric vehicle charging scheduling in a power distribution network. *IEEE Transactions on Smart Grid* 12, 1416–1428. doi:[10.1109/TSG.2020.3028470](https://doi.org/10.1109/TSG.2020.3028470).

Jin, R., Zhou, Y., Lu, C., Song, J., 2022. Deep reinforcement learning-based strategy for charging station participating in demand response. *Applied Energy* 328, 120140. URL: <https://www.sciencedirect.com/science/article/pii/S0306261922013976>, doi:<https://doi.org/10.1016/j.apenergy.2022.120140>.

Kamrani, A.S., Dini, A., Dagdougui, H., Sheshyekani, K., 2025. Multi-agent deep reinforcement learning with online and fair optimal dispatch of ev aggregators. *Machine Learning with Applications* , 100620URL: <https://www.sciencedirect.com/science/article/pii/S266682702500039>, doi:<https://doi.org/10.1016/j.mlwa.2025.100620>.

Kipf, T.N., Welling, M., 2016. Semi-supervised classification with graph convolutional networks. [arXiv:1609.02907](https://arxiv.org/abs/1609.02907).

Konstantakopoulos, G.D., Gayialis, S.P., Kechagias, E.P., 2022. Vehicle routing problem and related algorithms for logistics distribution: a literature review and classification. *Operational Research* 22, 2033–2062. URL: <https://doi.org/10.1007/s12351-020-00600-7>, doi:[10.1007/s12351-020-00600-7](https://doi.org/10.1007/s12351-020-00600-7).

Lai, Y., Liu, J., Tang, Z., Wang, B., Hao, J., Luo, P., 2023. ChiPFormer: Transferable chip placement via offline decision transformer, in: Krause, A., Brunskill, E., Cho, K., Engelhardt, B., Sabato, S., Scarlett, J. (Eds.), *Proceedings of the 40th International Conference on Machine Learning*, PMLR. pp. 18346–18364. URL: <https://proceedings.mlr.press/v202/lai23c.html>.

Lan, Q., Mahmood, A.R., Yan, S., Xu, Z., 2023. Learning to optimize for reinforcement learning. [arXiv:2302.01470](https://arxiv.org/abs/2302.01470).

Lee, K.H., Nachum, O., Yang, M., Lee, L., Freeman, D., Xu, W., Guadarrama, S., Fischer, I., Jang, E., Michalewski, H., Mordatch, I., 2024. Multi-game decision transformers, in: *Proceedings of the 36th International Conference on Neural Information Processing Systems*, Curran Associates Inc., Red Hook, NY, USA.

Levine, S., Kumar, A., Tucker, G., Fu, J., 2020. Offline reinforcement learning: Tutorial, review, and perspectives on open problems. [arXiv:2005.01643](https://arxiv.org/abs/2005.01643).

Li, S., Hu, W., Cao, D., Dragičević, T., Huang, Q., Chen, Z., Blaabjerg, F., 2022. Electric vehicle charging management based on deep reinforcement learning. *Journal of Modern Power Systems and Clean Energy* 10, 719–730. doi:[10.35833/MPC.2020.000460](https://doi.org/10.35833/MPC.2020.000460).

Liu, Z., Guo, Z., Yao, Y., Cen, Z., Yu, W., Zhang, T., Zhao, D., 2023. Constrained decision transformer for offline safe reinforcement learning. [arXiv:2302.07351](https://arxiv.org/abs/2302.07351).

Orfanoudakis, S., Diaz-Londono, C., Emre Yilmaz, Y., Palensky, P., Vergara, P.P., 2025a. Ev2gym: A flexible v2g simulator for ev smart charging research and benchmarking. *IEEE Transactions on Intelligent Transportation Systems* 26, 2410–2421.

Orfanoudakis, S., Robu, V., Salazar, E.M., Palensky, P., Vergara, P.P., 2025b. Scalable reinforcement learning for large-scale coordination of electric vehicles using graph neural networks.

Panda, N.K., Tindemans, S.H., 2024. Quantifying the aggregate flexibility of ev charging stations for dependable congestion management products: A dutch case study. [arXiv:2403.13367](https://arxiv.org/abs/2403.13367).

Paster, K., McIlraith, S.A., Ba, J., 2024. You can't count on luck: why decision transformers and rvs fail in stochastic environments, in: Proceedings of the 36th International Conference on Neural Information Processing Systems, Curran Associates Inc., Red Hook, NY, USA.

Qiu, D., Wang, Y., Hua, W., Strbac, G., 2023. Reinforcement learning for electric vehicle applications in power systems:a critical review. Renewable and Sustainable Energy Reviews 173, 113052. URL: <https://www.sciencedirect.com/science/article/pii/S1364032122009339>, doi:<https://doi.org/10.1016/j.rser.2022.113052>.

Raffin, A., Hill, A., Gleave, A., Kanervisto, A., Ernestus, M., Dormann, N., 2021. Stable-baselines3: Reliable reinforcement learning implementations. Journal of Machine Learning Research 22, 1–8. URL: <http://jmlr.org/papers/v22/20-1364.html>.

Roald, L.A., Pozo, D., Papavasiliou, A., Molzahn, D.K., Kazempour, J., Conejo, A., 2023. Power systems optimization under uncertainty: A review of methods and applications. Electric Power Systems Research 214, 108725. URL: <https://www.sciencedirect.com/science/article/pii/S0378779622007842>, doi:<https://doi.org/10.1016/j.epsr.2022.108725>.

Sadeghianpourhamami, N., Deleu, J., Develder, C., 2020. Definition and evaluation of model-free coordination of electrical vehicle charging with reinforcement learning. IEEE Transactions on Smart Grid 11, 203–214. doi:[10.1109/TSG.2019.2920320](https://doi.org/10.1109/TSG.2019.2920320).

Seno, T., Imai, M., 2022. d3rlpy: An offline deep reinforcement learning library. Journal of Machine Learning Research 23, 1–20. URL: <http://jmlr.org/papers/v23/22-0017.html>.

Sutton, R.S., Barto, A.G., 2018. Reinforcement learning: An introduction. MIT press.

Veličković, P., Cucurull, G., Casanova, A., Romero, A., Liò, P., Bengio, Y., 2018. Graph attention networks. URL: <https://arxiv.org/abs/1710.10903>, arXiv:1710.10903.

Villarrubia-Martin, E., Rodriguez-Benitez, L., Jimenez-Linares, L., Muñoz-Valero, D., Liu, J., 2023. A hybrid online off-policy reinforcement learning agent framework supported by transformers. International Journal of Neural Systems 33. doi:[10.1142/s012906572350065x](https://doi.org/10.1142/s012906572350065x).

Wang, B., 2024. Domain Adaptation in Reinforcement Learning: Approaches, Limitations, and Future Directions. Journal of The Institution of Engineers (India): Series B 105, 1223–1240. URL: <https://doi.org/10.1007/s40031-024-01049-4>, doi:[10.1007/s40031-024-01049-4](https://doi.org/10.1007/s40031-024-01049-4).

Wang, R., Foster, D.P., Kakade, S.M., 2020. What are the statistical limits of offline rl with linear function approximation? [arXiv:2010.11895](https://arxiv.org/abs/2010.11895).

Wu, Y.H., Wang, X., Hamaya, M., 2024. Elastic decision transformer, in: Proceedings of the 37th International Conference on Neural Information Processing Systems, Curran Associates Inc., Red Hook, NY, USA.

Yilmaz, Y.E., Orfanoudakis, S., Vergara, P.P., 2024. Reinforcement learning for optimized ev charging through power setpoint tracking, in: 2024 IEEE PES Innovative Smart Grid Technologies Europe (ISGT EUROPE), pp. 1–5.

Zhang, J., Liu, C., Li, X., Zhen, H.L., Yuan, M., Li, Y., Yan, J., 2023a. A survey for solving mixed integer programming via machine learning. Neurocomputing 519, 205–217. URL: <https://www.sciencedirect.com/science/article/pii/S0925231222014035>, doi:<https://doi.org/10.1016/j.neucom.2022.11.024>.

Zhang, S., Jia, R., Pan, H., Cao, Y., 2023b. A safe reinforcement learning-based charging strategy for electric vehicles in residential microgrid. Applied Energy 348, 121490. URL: <https://www.sciencedirect.com/science/article/pii/S0306261923008541>, doi:<https://doi.org/10.1016/j.apenergy.2023.121490>.

Zhang, Z., Mei, H., Xu, Y., 2023c. Continuous-time decision transformer for healthcare applications. Proceedings of Machine Learning Research 206, 6245–6262.

Zheng, Q., Zhang, A., Grover, A., 2022. Online decision transformer, in: Chaudhuri, K., Jegelka, S., Song, L., Szepesvari, C., Niu, G., Sabato, S. (Eds.), Proceedings of the 39th International Conference on Machine Learning, PMLR. pp. 27042–27059. URL: <https://proceedings.mlr.press/v162/zheng22c.html>.